

Dynamically induced conformation depending on excited normal modes of fast oscillation

Yoshiyuki Y. Yamaguchi*

*Department of Applied Mathematics and Physics,
Graduate School of Informatics, Kyoto University, Kyoto 606-8501, Japan*

Tatsuo Yanagita

Department of Engineering Science, Osaka Electro-Communication University, Neyagawa 572-8530, Japan

Tetsuro Konishi

General Education Division, College of Engineering, Chubu University, Kasugai 487-8501, Japan

Mikito Toda

*Faculty Division of Natural Sciences, Research Group of Physics,
Nara Women's University, Kita-Uoya-Nishimachi, Nara 630-8506, Japan[†]
Graduate School of Information Science, University of Hyogo,
7-1-28 Minatojima-minamimachi, Chuo-ku, Kobe, Hyogo 650-0047, Japan and
Research Institute for Electronic Science, Hokkaido University,
Kita 20 Nishi 10, Kita-Ku, Sapporo 001-0020, Japan*

We present dynamical effects on conformation in a simple bead-spring model consisting of three beads connected by two stiff springs. The conformation defined by the bending angle between the two springs is determined not only by a given potential energy function depending on the bending angle, but also fast motion of the springs which constructs the effective potential. A conformation corresponding with a local minimum of the effective potential is hence called the dynamically induced conformation. We develop a theory to derive the effective potential by using multiple-scale analysis and the averaging method. A remarkable consequence is that the effective potential depends on the excited normal modes of the springs and amount of the spring energy. Efficiency of the obtained effective potential is numerically verified.

I. INTRODUCTION

Conformation is deeply connected with function. A typical example is a biomolecule whose conformation is crucial for binding a ligand [1–5]. Morphological computation [6–8] is another example, which can be found for instance as walking robots [9, 10]. Mechanical metamaterial [11] provides several examples like the Miura fold which exhibits negative Poisson's ratio [12].

Realization of conformations is usually associated with the minimum of a potential energy function. In addition to the potential function, dynamics sometimes contributes to construct an effective potential. A well-known example is the Kapitza pendulum [13, 14]: An inverted pendulum persists against the gravity by applying a rapidly oscillating external force, since the effective potential provides a local minimum at the inverted position.

We present another dynamical effect on conformation realized in autonomous Hamiltonian systems containing fast and slow motion. Consider a bead-spring model [15] consisting of three beads connected by two stiff springs. The conformation of this system can be identified with

the bending angle between the two springs. If the system has a bending potential which depends only on the bending angle, one may imagine that the bending angle goes to a local minimum of the bending potential. The conformation of this system is, however, determined by the effective potential which consists of the bending potential and contribution from the fast spring motion.

More precise description of the above phenomenon is as follows. First of all, the dynamical effect is comparable with the bending potential under the condition that large bending motion is sufficiently slow than the spring motion. The bending potential dominates the effective potential when the spring energy is sufficiently small. However, the dynamical effect enlarges as the spring energy increases, and a local minimum of the effective potential does not necessarily coincide with a local minimum of the bending potential. We call a conformation corresponding to a local minimum of the effective potential a dynamically induced conformation (DIC). Further interesting fact is that the effective potential depends on the excited normal modes of the springs in addition to the spring energy. The three-body bead-spring model has the two normal modes of the springs and each mode makes a different valley.

The three-body system is quite simple, and hence it is theoretically tractable and clearly shows DIC. The aim of this paper is to present the dynamical contribution to conformation in the three-body system. It is worth not-

* yyama@amp.i.kyoto-u.ac.jp

[†] Present position: Research fellow, Nara Women's University

ing that the bead-spring model mimics several systems: a polymer [15, 16], a microscopic artificial swimmer [17], a soft magnetic nanowire [18], and a semi-flexible macromolecule [19].

A theoretical analysis reveals that the essence of DIC is existence of multiple timescales, which is realized in the bead-spring model by stiff springs and slow bending motion. Appearance of multiple timescales is generic in nature. For instance, biomolecules have several forces of diverse strength as strong covalent bonds, intermediate hydrogen bonds, and weak van der Waals forces, and each of them has a characteristic timescale. DIC therefore enriches understanding of the origin of conformation change and its function.

A celebrated example of the dynamically constructed effective potential is found in the aforementioned Kapitza pendulum, and it has been studied in a wide range of fields [20–36]. The development of the Kapitza pendulum suggests that DIC will provide a large spectrum of applications. Nevertheless, we underline three crucial differences between DIC and the Kapitza pendulum. (i) The bead-spring model is autonomous and the effective potential is intrinsically determined, while one in the Kapitza pendulum can be controlled by the applied external force. (ii) The effective potential depends on the excited normal modes in the bead-spring model. (iii) The local minimum points of the effective potential may continuously move depending on the spring energy in the bead-spring model, while the local minimum created by the external vertical oscillation is fixed at the inverted position in the Kapitza pendulum.

This paper is organized as follows. The three-body bead-spring model is presented in Sec. II with the two important assumptions to have DIC. Following the assumptions, we develop in Sec. III a theory to describe slow bending motion by using a multiple-scale analysis [37] and the averaging method [38–40]. The theory provides the effective potential depending on the excited normal modes of the springs and amount of the spring energy. Examples of the effective potential are exhibited in Sec. IV so as to reveal the above dependency. Efficiency of the effective potential is examined through numerical simulations in Sec. V. The final section VI is devoted to summary and discussions.

II. MODEL

The three-body bead-spring model is sketched in Fig. 1. We assume that the beads move on a two-dimensional plane. The mass and the position of the j th bead are respectively denoted by m_j and $\mathbf{r}_j \in \mathbb{R}^2$. The Lagrangian of the model is expressed by

$$L = \frac{1}{2} \sum_{j=1}^3 m_j \|\dot{\mathbf{r}}_j\|^2 - V(\mathbf{r}_1, \mathbf{r}_2, \mathbf{r}_3), \quad (1)$$

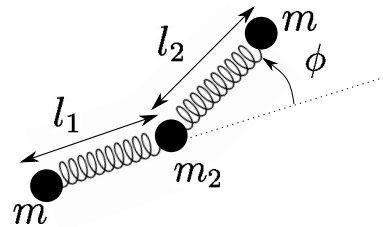


FIG. 1. The three-body bead-spring model. We assume the symmetric masses $m_1 = m_3 = m$ and the two springs having the identical potential.

where $\dot{\mathbf{r}}_j := d\mathbf{r}_j/dt$ and $\|\cdot\|$ is the Euclidean norm: $\|\mathbf{r}\| = \sqrt{x^2 + y^2}$ for $\mathbf{r} = (x, y) \in \mathbb{R}^2$. The j th and the $(j+1)$ th beads are connected by a stiff spring, and we assume that the two springs have the identical potential. Further, for simplicity, we focus on the symmetric masses: $m_1 = m_3 = m$. The term V represents the potential energy function, which will be specified later.

We assume that the system described by Eq. (1) has the two-dimensional translational symmetry and the rotational symmetry, which induce the conservation of the two-dimensional total momentum vector and of the total angular momentum, respectively. The total momentum vector can be set as the zero vector without loss of generality, while the total angular momentum is assumed to be zero. The three integrals reduce the system and the reduced Lagrangian is

$$L = \frac{1}{2} \sum_{\alpha, \beta=1}^3 C^{\alpha\beta}(\mathbf{y}) \dot{y}_\alpha \dot{y}_\beta - V(\mathbf{y}), \quad (2)$$

where

$$\mathbf{y} = (y_1, y_2, y_3)^T = (l_1, l_2, \phi)^T \quad (3)$$

and the superscript T represents transposition. The variables l_1 and l_2 are the lengths of the two springs,

$$l_j = \|\mathbf{r}_{j+1} - \mathbf{r}_j\|, \quad (j = 1, 2) \quad (4)$$

and ϕ is the bending angle,

$$\cos \phi = \frac{(\mathbf{r}_3 - \mathbf{r}_2) \cdot (\mathbf{r}_2 - \mathbf{r}_1)}{\|\mathbf{r}_3 - \mathbf{r}_2\| \|\mathbf{r}_2 - \mathbf{r}_1\|}, \quad (5)$$

where \cdot is the Euclidean inner product. The function $C^{\alpha\beta}(\mathbf{y})$ is the (α, β) element of the size-3 symmetric matrix $\mathbf{C}(\mathbf{y})$, whose explicit form is given in Appendix A. The potential energy function $V(\mathbf{y})$ consists of the two parts as

$$V(\mathbf{y}) = V_{\text{spring}}(l_1, l_2) + V_{\text{bend}}(\phi). \quad (6)$$

We call V_{spring} and V_{bend} the spring potential and the bending potential, respectively.

We introduce the two assumptions to realize DIC in the above model. Let ϵ be a dimensionless small parameter as $|\epsilon| \ll 1$. The two assumptions are:

(A1) The amplitudes of the springs are sufficiently small comparing with the natural length. The ratio is of $O(\epsilon)$.

(A2) Large bending motion is sufficiently slow than the spring motion. The ratio of the two timescales is of $O(\epsilon)$.

These two assumptions lead the effective potential for the bending angle ϕ . A local minimum point of the effective potential does not necessarily coincide with a local minimum point of the bending potential $V_{\text{bend}}(\phi)$. That is, the bending angle oscillates around an angle at which the bending potential $V_{\text{bend}}(\phi)$ does not take a local minimum. We develop a theory to derive the effective potential in Sec.III.

III. THEORY

From now on, we use the Einstein notation for the sum: We take the sum over an index if it appears twice in a term. We derive the equation of motion for the slow bending motion, and construct the effective potential induced by the fast spring motion. A review of the Kapitza pendulum is provided in Appendix B, which might be helpful to understand the theory.

A. Multiscale analysis and averaging

The Euler-Lagrange equations derived from Eq. (2) are

$$C^{\alpha\beta}(\mathbf{y})\ddot{y}_\beta + \left[\frac{\partial C^{\alpha\beta}}{\partial y_\gamma}(\mathbf{y}) - \frac{1}{2} \frac{\partial C^{\beta\gamma}}{\partial y_\alpha}(\mathbf{y}) \right] \dot{y}_\beta \dot{y}_\gamma + \frac{\partial V}{\partial y_\alpha}(\mathbf{y}) = 0, \quad (7)$$

where $\alpha, \beta, \gamma \in \{1, 2, 3\}$. These equations are the starting point of our theory.

The assumption (A2) induces the two timescales of $t_0 = t$ and $t_1 = \epsilon t$. The fast timescale t_0 describes the fast spring motion, and the slow timescale t_1 corresponds to the slow bending motion. The two timescales transform the time derivative into

$$\frac{d}{dt} = \frac{\partial}{\partial t_0} + \epsilon \frac{\partial}{\partial t_1}. \quad (8)$$

From the assumptions (A1) and (A2) the variables l_j and ϕ are expanded as

$$\begin{cases} l_j(t_0, t_1) = l_j^{(0)} + \epsilon l_j^{(1)}(t_0, t_1), & l_j^{(0)} = l_* \quad (j = 1, 2) \\ \phi(t_0, t_1) = \phi^{(0)}(t_1) + \epsilon \phi^{(1)}(t_0, t_1), \end{cases} \quad (9)$$

where l_* is the natural length of the two springs. As we will observe later, the fast motion of $\phi^{(1)}(t_0, t_1)$ is induced by the fast motion of the springs and is of the same order $O(\epsilon)$ as the spring amplitudes. We are interested in

$\phi^{(0)}(t_1)$, which represents large and slow bending motion. We denote the above expansions for simplicity as

$$\mathbf{y}(t_0, t_1) = \mathbf{y}^{(0)}(t_1) + \epsilon \mathbf{y}^{(1)}(t_0, t_1). \quad (10)$$

We further expand the potential energy function V . The spring potential V_{spring} is assumed to be expanded into the Taylor series around the natural length as

$$V_{\text{spring}}(l_1, l_2) = \frac{k}{2} \sum_{j=1}^2 (l_j - l_*)^2 + O(|l_j - l_*|^3). \quad (11)$$

That is, the two springs have the same spring constant

$$k = \frac{\partial^2 V_{\text{spring}}}{\partial l_j^2}(l_*, l_*). \quad (j = 1, 2). \quad (12)$$

The bending potential is assumed to be expanded into the series of ϵ as

$$V_{\text{bend}}(\phi) = V_{\text{bend}}^{(0)}(\phi) + \epsilon V_{\text{bend}}^{(1)}(\phi) + \epsilon^2 V_{\text{bend}}^{(2)}(\phi) + \dots \quad (13)$$

The two assumptions (A1) and (A2) induce

$$V_{\text{bend}}^{(0)}(\phi), V_{\text{bend}}^{(1)}(\phi) \equiv 0 \quad (14)$$

as shown in Appendix C, and hence the leading term of V_{bend} is of $O(\epsilon^2)$. This ordering results from the assumption (A2): The force from the bending potential V_{bend} should be weaker than that of the spring potential V_{spring} .

We construct the equations of motion order by order, by substituting Eqs. (8), (10), (11), and (13) into Eq. (7). In $O(\epsilon^0)$, we have no terms, because $\partial y_\beta^{(0)}/\partial t_0 = 0$, $\dot{y}_\beta, \ddot{y}_\beta = O(\epsilon)$, and $\partial V/\partial y_\alpha = O(\epsilon)$.

In $O(\epsilon)$ we have

$$\frac{\partial^2 \mathbf{y}^{(1)}}{\partial t_0^2} = -\mathbf{X}(\mathbf{y}^{(0)})\mathbf{y}^{(1)}. \quad (15)$$

The size-3 matrix \mathbf{X} is defined by

$$\mathbf{X}(\mathbf{y}) = [\mathbf{C}(\mathbf{y})]^{-1} \mathbf{K}, \quad (16)$$

where

$$\mathbf{K} = \begin{pmatrix} k & 0 & 0 \\ 0 & k & 0 \\ 0 & 0 & 0 \end{pmatrix}. \quad (17)$$

See Appendix D for the explicit form of $\mathbf{X}(\mathbf{y}^{(0)})$. The third column vector of \mathbf{X} is the zero vector, and the right-hand side of Eq. (15) has no contribution from the third element of $\mathbf{y}^{(1)}$, namely $\phi^{(1)}$. The fast motion of $\phi^{(1)}$ is hence induced by $l_1^{(1)}$ and $l_2^{(1)}$, as mentioned after Eq. (9).

The slow motion of $\phi^{(0)}(t_1)$ is described in $O(\epsilon^2)$, and the equation of motion for $\phi^{(0)}(t_1)$ is

$$\begin{aligned} C^{3\beta}(\mathbf{y}^{(0)})(\ddot{y}_\beta)^{(2)} + \left[\frac{\partial C^{3\beta}}{\partial y_\gamma}(\mathbf{y}^{(0)}) - \frac{1}{2} \frac{\partial C^{\beta\gamma}}{\partial \phi}(\mathbf{y}^{(0)}) \right] (\dot{y}_\beta)^{(1)}(\dot{y}_\gamma)^{(1)} \\ + \frac{\partial C^{3\beta}}{\partial y_\gamma}(\mathbf{y}^{(0)})(\ddot{y}_\beta)^{(1)}y_\gamma^{(1)} + \frac{dV_{\text{bend}}^{(2)}}{d\phi}(\phi^{(0)}) = 0. \end{aligned} \quad (18)$$

Here $(\dot{\mathbf{y}})^{(1)}$ is the first order part of $\dot{\mathbf{y}}$ and $(\dot{\mathbf{y}})^{(1)} \neq d\mathbf{y}^{(1)}/dt$. The explicit forms are

$$\begin{aligned} (\dot{\mathbf{y}})^{(1)} &= \frac{d\mathbf{y}^{(0)}}{dt_1} + \frac{\partial \mathbf{y}^{(1)}}{\partial t_0}, \\ (\ddot{\mathbf{y}})^{(1)} &= \frac{\partial^2 \mathbf{y}^{(1)}}{\partial t_0^2}, \\ (\ddot{\mathbf{y}})^{(2)} &= \frac{d^2 \mathbf{y}^{(0)}}{dt_1^2} + 2 \frac{\partial^2 \mathbf{y}^{(1)}}{\partial t_0 \partial t_1}. \end{aligned} \quad (19)$$

Equation (18) contains the fast oscillation of $\mathbf{y}^{(1)}$, and we eliminate it by taking the average over the fast timescale t_0 . The average is defined by

$$\langle \varphi \rangle (t_1) = \lim_{T \rightarrow \infty} \frac{1}{T} \int_0^T \varphi(t_0, t_1) dt_0 \quad (20)$$

for an arbitrary function $\varphi(t_0, t_1)$. After taking the average and recalling $\mathbf{y}^{(0)} = (l_*, l_*, \phi^{(0)})$, Eq. (18) is simplified to

$$\begin{aligned} C^{33}(\mathbf{y}^{(0)}) \frac{d^2 \phi^{(0)}}{dt_1^2} + \frac{1}{2} \frac{\partial C^{33}}{\partial \phi}(\mathbf{y}^{(0)}) \left(\frac{d\phi^{(0)}}{dt_1} \right)^2 \\ = - \frac{dV_{\text{bend}}^{(2)}}{d\phi}(\phi^{(0)}) + \mathcal{A}. \end{aligned} \quad (21)$$

The right-hand side represents the force, and the averaged term

$$\mathcal{A} = \frac{1}{2} \text{Tr} \left[\frac{\partial \mathbf{C}}{\partial \phi}(\mathbf{y}^{(0)}) \left\langle \frac{\partial \mathbf{y}^{(1)}}{\partial t_0} \left(\frac{\partial \mathbf{y}^{(1)}}{\partial t_0} \right)^T \right\rangle \right] \quad (22)$$

represents the effective force yielded by the fast spring motion. Here Tr represents the matrix trace. The right-hand side of Eq. (22) depends on $\mathbf{y}^{(0)}$ and $\mathbf{y}^{(1)}$. The $\mathbf{y}^{(0)}$ dependence can be regarded as the $\phi^{(0)}$ dependence, since $\mathbf{y}^{(0)} = (l_*, l_*, \phi^{(0)})$ and l_* is constant. $\mathbf{y}^{(1)}$ depends on t_0 and t_1 , and the t_0 dependence is averaged out. We have to eliminate the t_1 dependence to obtain the effective potential as a function of $\phi^{(0)}$.

B. Explicit form of the averaged term

We compute the explicit form of the averaged term \mathcal{A} by performing the diagonalization of Eq. (15), and observe the t_1 dependence, which has to be eliminated. Let \mathbf{P} diagonalize \mathbf{X} as

$$\mathbf{X}(\mathbf{y}^{(0)}) \mathbf{P}(\mathbf{y}^{(0)}) = \mathbf{P}(\mathbf{y}^{(0)}) \mathbf{\Lambda}(\mathbf{y}^{(0)}). \quad (23)$$

The diagonal matrix $\mathbf{\Lambda}(\mathbf{y}^{(0)})$ consists of the eigenvalues of $\mathbf{X}(\mathbf{y}^{(0)})$ and is denoted by

$$\mathbf{\Lambda}(\mathbf{y}^{(0)}) = \begin{pmatrix} \lambda_1(\mathbf{y}^{(0)}) & 0 & 0 \\ 0 & \lambda_2(\mathbf{y}^{(0)}) & 0 \\ 0 & 0 & 0 \end{pmatrix}, \quad (24)$$

where

$$\begin{aligned} \lambda_1(\mathbf{y}^{(0)}) &= \frac{k(M_2 - M_1 \cos \phi^{(0)})}{M_2^2 - M_1^2}, \\ \lambda_2(\mathbf{y}^{(0)}) &= \frac{k(M_2 + M_1 \cos \phi^{(0)})}{M_2^2 - M_1^2}, \end{aligned} \quad (25)$$

and

$$M_2 = \frac{m(m+m_2)}{2m+m_2}, \quad M_1 = \frac{m^2}{2m+m_2}. \quad (26)$$

A diagonalizing matrix is

$$\mathbf{P}(\mathbf{y}^{(0)}) = (\mathbf{p}_{\text{in}}, \mathbf{p}_{\text{anti}}, \mathbf{p}_{\phi}) = \begin{pmatrix} 1/\sqrt{2} & 1/\sqrt{2} & 0 \\ 1/\sqrt{2} & -1/\sqrt{2} & 0 \\ v(\mathbf{y}^{(0)}) & 0 & 1 \end{pmatrix} \quad (27)$$

with

$$v(\mathbf{y}^{(0)}) = \frac{\sqrt{2}}{l_*} \frac{M_1 \sin \phi^{(0)}}{M_2 - M_1 \cos \phi^{(0)}}. \quad (28)$$

The three column vectors \mathbf{p}_{in} , \mathbf{p}_{anti} , and \mathbf{p}_{ϕ} are eigenvectors of $\mathbf{X}(\mathbf{y}^{(0)})$, and we call the three modes as the in-phase mode, the anti-phase mode, and the zero-eigenvalue mode, respectively.

To solve Eq. (15), we perform the change of variables as

$$\mathbf{y}^{(1)} = \mathbf{P}(\mathbf{y}^{(0)}) \boldsymbol{\eta}, \quad (29)$$

and $\boldsymbol{\eta}$ solves the diagonalized equations

$$\frac{\partial^2 \boldsymbol{\eta}}{\partial t_0^2} = -\mathbf{\Lambda}(\mathbf{y}^{(0)}) \boldsymbol{\eta}. \quad (30)$$

Denoting the amplitudes of the in-phase and the anti-phase modes by $w_1(t_1)$ and $w_2(t_1)$ respectively, which evolve in the slow timescale t_1 through the coupling with $\phi^{(0)}(t_1)$, and setting the amplitude of the zero-eigenvalue mode as zero, we introduce the diagonal matrix

$$\mathbf{W}(t_1) = \begin{pmatrix} w_1(t_1) & 0 & 0 \\ 0 & w_2(t_1) & 0 \\ 0 & 0 & 0 \end{pmatrix}. \quad (31)$$

Putting all together and remembering that the average of the square of a sinusoidal function is 1/2, we have

$$\begin{aligned} \mathcal{A}(\phi^{(0)}, w_1, w_2) &= \frac{1}{4} \text{Tr} \left[\frac{\partial \mathbf{C}}{\partial \phi}(\mathbf{y}^{(0)}) \mathbf{P} \mathbf{\Lambda} \mathbf{W}^2 \mathbf{P}^T \right] \\ &= -\frac{k}{4} \left[\frac{M_1 \sin \phi^{(0)}}{M_2 - M_1 \cos \phi^{(0)}} w_1^2 - \frac{M_1 \sin \phi^{(0)}}{M_2 + M_1 \cos \phi^{(0)}} w_2^2 \right]. \end{aligned} \quad (32)$$

The averaged term \mathcal{A} contains the two evolving amplitudes $w_1(t_1)$ and $w_2(t_1)$. The untrivial evolution of the amplitudes differs from the Kapitza pendulum, which also contains the amplitude of the external oscillation but it is explicitly given. We have to eliminate the two unknown amplitudes from the averaged term \mathcal{A} to obtain a closed equation for $\phi^{(0)}(t_1)$.

C. Hypothesis and energy conservation

The strategy to eliminate the two unknown amplitudes $w_1(t_1)$ and $w_2(t_1)$ is as follows. First, we introduce a hypothesis, which is inspired from the adiabatic invariant. The hypothesis reduces the number of unknown variables from two to one. Second, we eliminate the remaining unknown variable by using the energy conservation law.

The first step is the introduction of the hypothesis expressed by

$$(H) \quad w_1(t_1)^2 = \nu_1 w(t_1)^2, \quad w_2(t_1)^2 = \nu_2 w(t_1)^2, \quad (33)$$

where ν_1 and ν_2 are constants satisfying

$$\nu_1 + \nu_2 = 1. \quad (34)$$

A physical interpretation of the hypothesis (H) is that the slow bending motion exchanges energy with the fast spring motion in proportion to its normal mode energy. Validity of the hypothesis (H) is examined in Appendix E. We note that the hypothesis should be valid if the modification of $\phi^{(0)}$ is sufficiently small. The unique unknown variable is now $w(t_1)$, while the constants ν_1 and ν_2 have been included in the equations of motion.

The second step is the energy conservation. The leading order of the total energy is of $O(\epsilon^2)$ and we expand it as $E = \epsilon^2 E^{(2)} + O(\epsilon^3)$. The leading term is

$$E^{(2)} = \frac{1}{2} \text{Tr} \left[\mathbf{C}(\mathbf{y}^{(0)}) (\dot{\mathbf{y}}^{(1)}) (\dot{\mathbf{y}}^{(1)})^T \right] + \frac{1}{2} \text{Tr} \left[\mathbf{K} \mathbf{y}^{(1)} \mathbf{y}^{(1)T} \right] + V_{\text{bend}}^{(2)}(\phi^{(0)}). \quad (35)$$

Taking the average over t_0 , we have

$$\langle E^{(2)} \rangle = \frac{1}{2} \text{Tr} \left[\mathbf{C}(\mathbf{y}^{(0)}) \frac{d\mathbf{y}^{(0)}}{dt_1} \left(\frac{d\mathbf{y}^{(0)}}{dt_1} \right)^T \right] + \frac{k}{2} \text{Tr} \mathbf{W}^2 + V_{\text{bend}}^{(2)}(\phi^{(0)}). \quad (36)$$

Substituting Eq. (33), the unique unknown variable w is obtained as

$$kw(t_1)^2 = 2 \left[E^{(2)} - V_{\text{bend}}^{(2)}(\phi^{(0)}) \right] - C^{33}(\mathbf{y}^{(0)}) \left(\frac{d\phi^{(0)}}{dt_1} \right)^2, \quad (37)$$

where we denoted $\langle E^{(2)} \rangle$ by $E^{(2)}$ for simplicity. Finally, we eliminate the unknown amplitudes from the averaged term \mathcal{A} represented in Eq. (32) by substituting Eqs. (33) and (37):

$$\mathcal{A}(\phi^{(0)}) = \left[\frac{E^{(2)} - V_{\text{bend}}^{(2)}(\phi^{(0)})}{2} - \frac{1}{4} C^{33}(\mathbf{y}^{(0)}) \left(\frac{d\phi^{(0)}}{dt_1} \right)^2 \right] T_\nu, \quad (38)$$

where

$$T_\nu = - \left[\frac{M_1 \sin \phi^{(0)}}{M_2 - M_1 \cos \phi^{(0)}} \nu_1 - \frac{M_1 \sin \phi^{(0)}}{M_2 + M_1 \cos \phi^{(0)}} \nu_2 \right]. \quad (39)$$

We underline that the averaged term \mathcal{A} depends on the constants ν_1, ν_2 and $E^{(2)}$.

D. Final result

Substituting Eq. (38) into Eq. (21), we have

$$\frac{d^2 \phi^{(0)}}{dt_1^2} + F_\nu(\phi^{(0)}) \left(\frac{d\phi^{(0)}}{dt_1} \right)^2 + G_\nu(\phi^{(0)}) = 0 \quad (40)$$

where

$$F_\nu(\phi^{(0)}) = \frac{1}{2C^{33}(\mathbf{y}^{(0)})} \frac{\partial C^{33}}{\partial \phi}(\mathbf{y}^{(0)}) + \frac{1}{4} T_\nu, \quad (41)$$

$$G_\nu(\phi^{(0)}) = \frac{1}{C^{33}(\mathbf{y}^{(0)})} \left[\frac{dV_{\text{bend}}^{(2)}}{d\phi}(\phi^{(0)}) - \frac{E^{(2)} - V_{\text{bend}}^{(2)}(\phi^{(0)})}{2} T_\nu \right], \quad (42)$$

and

$$C^{33}(\phi^{(0)}) = \frac{l_*^2}{2} (M_2 - M_1 \cos \phi^{(0)}). \quad (43)$$

Equation (40) is the closed equation for the slow bending motion. It is reproduced as the Euler-Lagrange equation of the effective Lagrangian

$$L_{\text{eff}} \left(\phi^{(0)}, \frac{d\phi^{(0)}}{dt_1} \right) = \frac{1}{2} M_{\text{eff}}(\phi^{(0)}) \left(\frac{d\phi^{(0)}}{dt_1} \right)^2 - V_{\text{eff}}(\phi^{(0)}). \quad (44)$$

Here, the effective (dimensionless) mass $M_{\text{eff}}(\phi^{(0)})$ is

$$M_{\text{eff}}(\phi^{(0)}) = \exp \left[2 \int_0^{\phi^{(0)}} F_\nu(z) dz \right] = \left(\frac{M_2 - M_1 \cos \phi^{(0)}}{M_2 - M_1} \right)^{1-\nu_1/2} \left(\frac{M_2 + M_1}{M_2 + M_1 \cos \phi^{(0)}} \right)^{\nu_2/2}, \quad (45)$$

and the effective potential $V_{\text{eff}}(\phi^{(0)})$ is

$$V_{\text{eff}}(\phi^{(0)}) = \int_0^{\phi^{(0)}} M_{\text{eff}}(z) G_\nu(z) dz. \quad (46)$$

Note that the physical dimension of V_{eff} differs from $V_{\text{bend}}^{(2)}$ due to the factor $1/C^{33}$.

The effective potential V_{eff} of Eq. (46) is the main product of the theory. A remarkable observation is that V_{eff} depends on energy $E^{(2)}$ and the normal mode energy distribution (ν_1, ν_2) through M_{eff} [Eq. (45)] and G_ν [Eq. (42)]. Examples of the effective potential are exhibited in Sec. IV.

IV. EFFECTIVE POTENTIAL

We exhibit examples of the effective potential with varying the parameters $E^{(2)}$ and ν_1 (remember $\nu_2 = 1 - \nu_1$). The equal mass condition $m_2 = m$ is assumed unless there is a notice. Note that the in-phase (anti-phase) mode is the mode-1 (mode-2) as defined in Sec. III B.

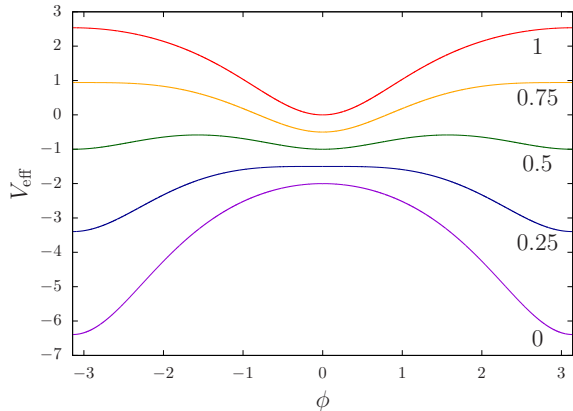


FIG. 2. The effective potential $V_{\text{eff}}(\phi)$. $V_{\text{bend}} \equiv 0$. The numbers in the panels represent the values of ν_1 , while $\nu_2 = 1 - \nu_1$. The total energy $E^{(2)}$ is an overall factor of V_{eff} and is set as $E^{(2)} = 1$. Graphs are shifted in the vertical direction by a graphical reason.

A. Examples without bending potential

First of all, we observe the effective potential V_{eff} without bending potential, $V_{\text{bend}} \equiv 0$, to observe the simplest case. We exhibit effective potentials for some values of ν_1 ($\nu_2 = 1 - \nu_1$) in Fig. 2. The dynamical contribution is completely opposite between the in-phase mode and the anti-phase mode. The in-phase mode makes a valley at $\phi = 0$, while the anti-phase mode makes a valley at $\phi = \pi$. A precise analysis reveals that there are the two local minima at $\phi = 0$ and π in the interval of $\nu_1 \in (1/4, 3/4)$. The coexistence interval is generalized to

$$\nu_1 \in \left(\frac{M_2 - M_1}{2M_2}, \frac{M_2 + M_1}{2M_2} \right) \quad (47)$$

for any value of m_2 . See Appendix F for details.

B. Examples with a bending potential

Next, we introduce an example of the bending potential as

$$V_{\text{bend}}^{(2)}(\phi) = \cos 2\phi + 1. \quad (48)$$

This potential has the two minima at $\phi = \pm\pi/2$. We set the equal mass condition, $m_2 = m$. Since V_{eff} depends on the normal mode energy distribution (ν_1, ν_2) and the total energy $E^{(2)}$, we show graphs of the effective potential for $(\nu_1, \nu_2) = (1, 0)$ (in-phase), $(1/2, 1/2)$ (mixed), and $(0, 1)$ (anti-phase) with varying the value of $E^{(2)}$ in Fig. 3. The effective potential V_{eff} is similar to the bending potential $V_{\text{bend}}^{(2)}$ when the total energy $E^{(2)}$ is small. As the total energy increases, the local minimum points move from $\phi = \pm\pi/2$ towards $\phi = 0$ and/or $\phi = \pi$. The

local minimum points of V_{eff} are the dynamically induced conformations (DICs).

The effective potential is determined at each point on the $(E^{(2)}, \nu_1)$ plane, and yields the set of the local minimum points. We categorize the local minimum points into the three classes: $\phi = 0, \pi$, and $\phi_{\sharp} (\neq 0, \pi)$. The three classes induce the seven types of sets as arranged in Table I. By using the seven types, the $(E^{(2)}, \nu_1)$ plane is divided into regions each of which is assigned by a type of the set as reported in Fig. 4. We stress that the seven types are realized by changing the total energy $E^{(2)}$ and the mode energy distribution ν_1 .

TABLE I. The seven types of local minimum point sets of the effective potential V_{eff} . The symbol ϕ_{\sharp} represents a conformation which is neither $\phi = 0$ nor $\phi = \pi$. For each type the conformation ϕ with the symbol M (O) is a local minimum point (not a local minimum point).

Conformation ϕ	I	II ₀	II _{π}	III ₀	III _{π}	IV	V
$\phi_{\sharp} (\neq 0, \pi)$	M	O	O	M	M	O	M
0	O	M	O	M	O	M	M
π	O	O	M	O	M	M	M

Finally, we present a phase diagram by varying the center mass m_2 with fixing $E^{(2)} = 4$ in Fig. 5. We give two remarks. First, the seven types are also realized by changing the center mass m_2 . The regions assigned by the types III₀, III _{π} , IV, and V are enhanced comparing with Fig. 4. This fact suggests that the mass distribution is useful to control the conformation. Second, the dynamical contribution dominates the effective potential when m_2 is small. This domination can be explained from Eq. (39), which is a part of the averaged term \mathcal{A} , and Eq. (26), which is the definitions of M_2 and M_1 . We have $M_2 \rightarrow M_1$ as $m_2 \rightarrow 0$ from Eq. (26). Thus, the denominators of the function T_{ν} can be close to 0 near $\phi^{(0)} = 0, \pi$, and hence contribution from the averaged term becomes large.

V. NUMERICAL TESTS

We verify efficiency of the effective potential through numerical simulations of the model.

A. Setting

Numerical simulations are performed by using the fourth order symplectic integrator [42] for the Hamiltonian

$$H = \frac{1}{2} \sum_{j=1}^3 \frac{\|\mathbf{p}_j\|^2}{m_j} + V(\mathbf{r}_1, \mathbf{r}_2, \mathbf{r}_3), \quad \mathbf{p}_j = m_j \dot{\mathbf{r}}_j, \quad (49)$$

which is the Legendre transform of Eq. (1). The time step is set as $\Delta t = 10^{-3}$. The relative energy error

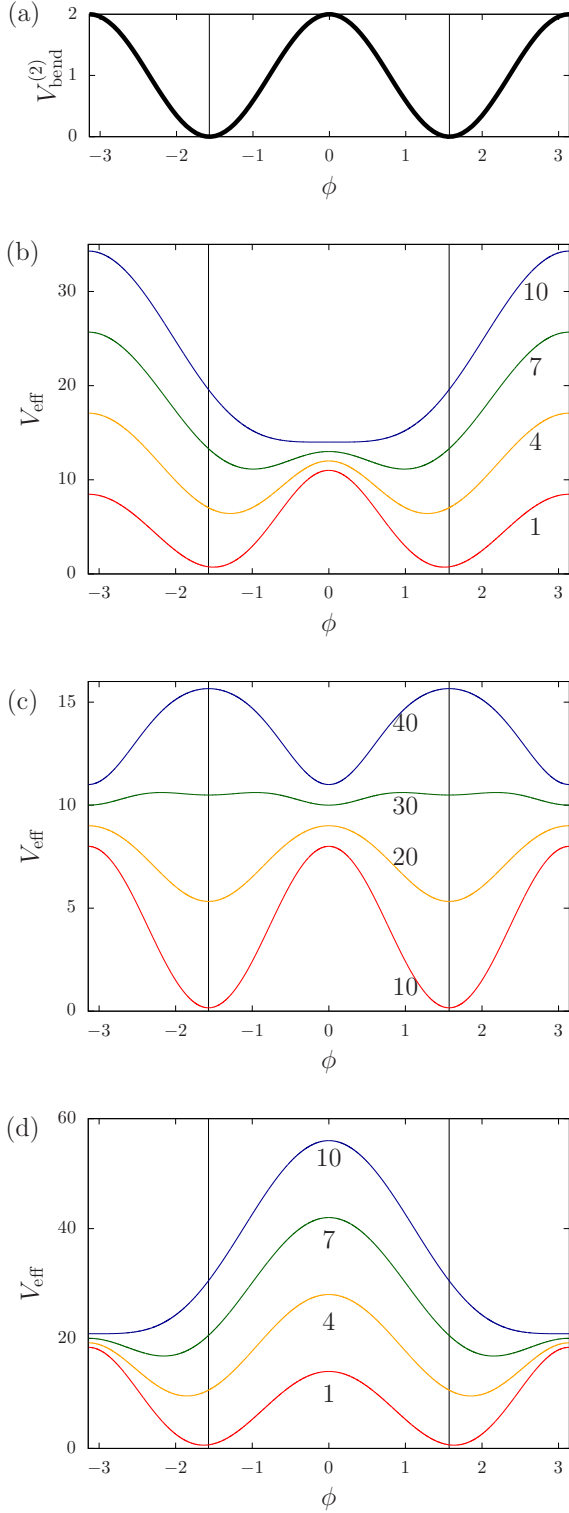


FIG. 3. The bending potential $V_{\text{bend}}^{(2)}(\phi) = 2 \cos \phi + 1$ (a) and the effective potential $V_{\text{eff}}(\phi)$ [(b)-(d)]. (b) $(\nu_1, \nu_2) = (1, 0)$ (the in-phase mode). (c) $(\nu_1, \nu_2) = (0.5, 0.5)$ (a mixed mode). (d) $(\nu_1, \nu_2) = (0, 1)$ (the anti-phase mode). The numbers in the panels (b)-(d) represent values of $E^{(2)}$. Graphs are shifted in the vertical direction by a graphical reason. The black vertical straight lines mark the minimum points of $V_{\text{bend}}^{(2)}(\phi)$.

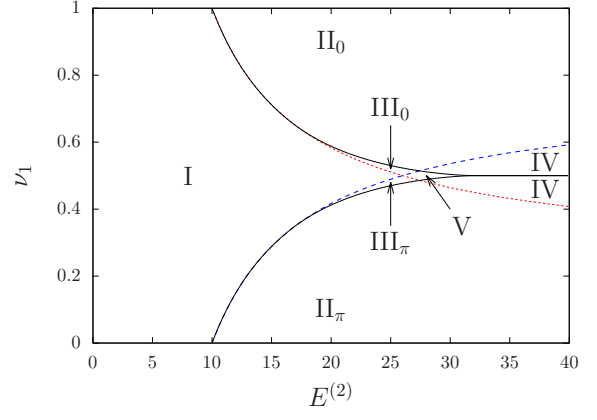


FIG. 4. The phase diagram on the $(E^{(2)}, \nu_1)$ plane with the equal mass condition $m_2 = m$. $m = 1$. $\nu_2 = 1 - \nu_1$. The effective potential takes a local minimum at $\phi = 0$ over the red dotted line, and at $\phi = \pi$ under the blue dashed line, where the two lines are obtained from Eqs. (F17) and (F18) respectively. $\phi = \phi_{\#}$ ($\neq 0, \pi$) is a local minimum point between the two solid black lines. See Table I for the types from I to V.

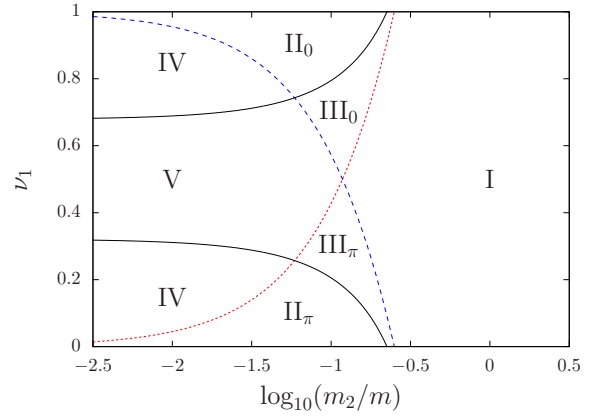


FIG. 5. The phase diagram on the plane $(m_2/m, \nu_1)$ with $E^{(2)} = 4$. The meanings of the lines are the same as Fig. 4. See Table I for the types from I to V.

is suppressed in the reported simulations as $|(E_{\text{num}} - E_0)/E_0| < 10^{-10}$, where E_0 and E_{num} are respectively the initial energy and the numerically obtained energy.

The two springs are assumed to be linear and V_{spring} is

$$V_{\text{spring}}(l_1, l_2) = \frac{k}{2} [(l_1 - l_*)^2 + (l_2 - l_*)^2], \quad (50)$$

because the theory includes only the linear part of the springs. The bending potential is $V_{\text{bend}} = \epsilon^2 V_{\text{bend}}^{(2)}$, and we use Eq. (48) as $V_{\text{bend}}^{(2)}$. The small parameter ϵ is fixed as $\epsilon = 0.1$. The masses are equal and $m_1 = m_2 = m_3 = m = 1$. The spring constant is $k = 10$, and the natural length is $l_* = 1$.

B. Initial condition

We set the initial condition as follows. All the beads have zero initial velocities in the x - and y -directions. The beads are once placed at the natural lengths of the springs with the bending angle ϕ_* . Then, under the hypothesis (H), we give small displacements of l_1, l_2 , and ϕ so as to excite the normal modes of the springs for a given pair of (ν_1, ν_2) . The initial condition, denoted by the subscript 0, is summarized as

$$\begin{cases} \begin{pmatrix} l_{1,0} \\ l_{2,0} \\ \phi_0 \end{pmatrix} = \begin{pmatrix} l_* \\ l_* \\ \phi_* \end{pmatrix} + \epsilon w \left[\sqrt{\nu_1} \mathbf{p}_{\text{in}}(\mathbf{y}^{(0)}) + \sqrt{\nu_2} \mathbf{p}_{\text{anti}} \right], \\ \begin{pmatrix} \dot{l}_{1,0} \\ \dot{l}_{2,0} \\ \dot{\phi}_0 \end{pmatrix} = \begin{pmatrix} 0 \\ 0 \\ 0 \end{pmatrix}. \end{cases} \quad (51)$$

See Eq. (27) for the definitions of \mathbf{p}_{in} and \mathbf{p}_{anti} . We note that the amplitude w is of $O(\epsilon^0)$. In the Hamiltonian system of Eq. (49), a corresponding initial condition is

$$\begin{cases} \mathbf{r}_{1,0} = \begin{pmatrix} -l_{1,0} \cos(\phi_0/2) \\ l_{1,0} \sin(\phi_0/2) \end{pmatrix}, \quad \mathbf{r}_{3,0} = \begin{pmatrix} l_{2,0} \cos(\phi_0/2) \\ l_{2,0} \sin(\phi_0/2) \end{pmatrix} \\ \mathbf{r}_{2,0} = \mathbf{p}_{1,0} = \mathbf{p}_{2,0} = \mathbf{p}_{3,0} = \mathbf{0}, \end{cases} \quad (52)$$

where $\mathbf{0}$ is the two-dimensional zero vector. The above initial condition gives the second order total energy as

$$E^{(2)} = \frac{k}{2} w^2 + V_{\text{bend}}^{(2)}(\phi_0). \quad (53)$$

In the next section we set $\phi_* = \pi/2$, which is a local minimum point of the bending potential V_{bend} . The initial condition Eq. (51) hence has two free parameters of the amplitude w , which is equivalent with $E^{(2)}$ through Eq. (53), and the normal mode energy ratio ν_1 (remember $\nu_2 = 1 - \nu_1$).

C. Efficiency of the effective potential

We concentrate on the in-phase mode, $(\nu_1, \nu_2) = (1, 0)$. Temporal evolution of $\phi(t)$ is exhibited in Figs. 6(d), (e), and (f) for three values of w , corresponding to three values of $E^{(2)}$ [see Eq. (53)]. Small and fast oscillation of $\phi(t)$ comes from $\phi^{(1)}$ and is induced from $l_j^{(1)}$, which are governed by Eq. (15). When the amplitude w is small, the bending angle ϕ almost stays around the initial value ϕ_0 [Fig. 6(d)], as it is predicted from the bending potential V_{bend} . However, the amplitude of oscillation of ϕ becomes large as w gets large, and the center of oscillation approaches to the zero [Figs. 6(e) and (f)]. We estimate the center of oscillation by the time average

$$\phi_{\text{ave}} = \frac{1}{T} \int_0^T \phi(t) dt, \quad T = 1000. \quad (54)$$

The estimated center is plotted as a function of $E^{(2)}$ in Fig. 6(g) with the minimum ϕ_{min} and the maximum ϕ_{max} of $\phi(t)$ in $t \in [0, 1000]$.

Two remarks are in order. First, the minimum and the maximum of ϕ are well predicted by V_{eff} . There is a gap between ϕ_{ave} and the bottom of V_{eff} in the energy interval approximated by $E^{(2)} \in [6.8, 10]$. The gap is not a counterevidence but a supporting evidence of the theory. This gap comes from the inequality $V_{\text{eff}}(0) < V_{\text{eff}}(\phi_0)$, which implies that the bending angle climbs over the saddle point at $\phi = 0$. This passing is confirmed by the jump of the theoretical minimum value of ϕ . Second, the center of oscillation is continuously modified as the spring energy increases. The conformation is determined not by a local minimum of the bending potential V_{bend} but by a local minimum of the effective potential V_{eff} derived from dynamics. We conclude that the effective potential successfully predicts the slow bending motion.

We provide movies in Supplemental Material [43] to show dynamics of the system. See Appendix G for explanation on the movies.

VI. SUMMARY AND DISCUSSIONS

We have investigated the three-body bead-spring model and demonstrated the dynamically induced conformation (DIC). The fast motion of the springs induces the effective potential for the slow bending motion, and the conformation is governed by the bottoms of the effective potential instead of the bending potential. One crucial remark is that the effective potential depends on the excited normal modes and its energy: The effective potential tends to have the minimum at $\phi = 0$ ($\phi = \pi$), by exciting the in-phase (anti-phase) mode. Moreover, a mixed mode makes the two local minima at $\phi = 0$ and π .

We have developed a theory to derive the effective potential based on the multiple-scale analysis and the averaging method. The main idea of the theory is to introduce a hypothesis inspired from the adiabatic invariant. The hypothesis with the energy conservation law eliminate the unknown variables being unavoidable in autonomous systems, and the elimination introduces the mode dependence and the total energy dependence into the effective potential. A theory for a generic system can be found in Refs. [44, 45].

Efficiency of the theoretically obtained effective potential is successfully examined through numerical simulations. The bending angle oscillates in general, and the center of oscillation is not a bottom of the bending potential, but a bottom of the effective potential. An extreme example is that a local maximum point of the bending potential becomes a local minimum point of the effective potential. The amplitude of the bending angle oscillation is also predicted by the effective potential.

The studied model is quite simple as we neglected the excluded volume effect, for instance. The potential of the excluded volume effect, and any other potentials be-

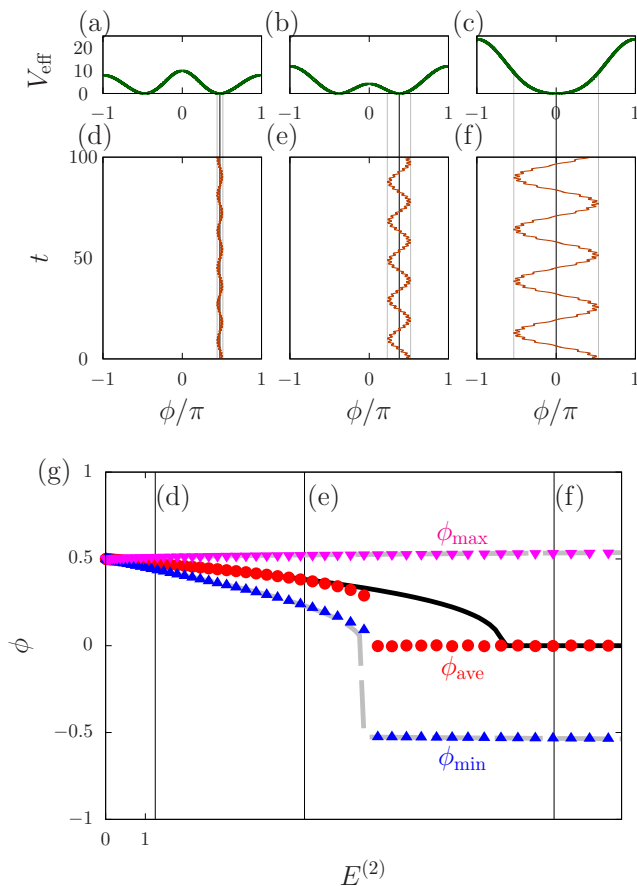


FIG. 6. Graphs of the effective potential [(a)-(c)] and temporal evolution of $\phi(t)$ with the reference conformation $\phi_* = \pi/2$ [(d)-(f)]. $(\nu_1, \nu_2) = (1, 0)$. The amplitude w is (a,d) $w = 0.5$, (b,e) $w = 1$, and (c,f) $w = 1.5$. The vertical black straight solid line represents the minimum point of V_{eff} . The two vertical gray straight dashed lines represent the two values of ϕ satisfying $V_{\text{eff}}(\phi) = V_{\text{eff}}(\phi_0)$ and belonging to the same valley. (g) Energy dependence of the time average ϕ_{ave} (red circles) with the minimum ϕ_{min} (blue triangles) and the maximum ϕ_{max} (purple inverse triangles) of ϕ in the time interval $t \in [0, 1000]$. The black solid and the gray dashed thick lines corresponds respectively to the vertical black and gray straight lines presented in the panels (d), (e), and (f). The three black vertical solid lines indicate the values of energy which correspond to the panels (d), (e), and (f) from left to right.

tween the two beads of the ends, can be treated in the same way as the bending potential discussed in this article (see Appendix H). Therefore, the phenomenon of DIC is universal as long as the two assumptions (A1) and (A2) hold.

We give three discussions on DIC revealed in this article: universality, application to control, and the beat effect. First, DIC must be universal since the essential mechanism to have DIC is existence of multiple timescales. Indeed, numerical simulations show that N -body bead-spring systems exhibit DIC [41]. Details will be reported elsewhere. Second, it is interesting to

use DIC for controlling the conformation of proteins by changing energy. Control of a robot is also an interesting subject by changing the center mass m_2 as shown in Fig. 5. Finally, we have neglected the beat effect between the eigenfrequencies of the fast springs, namely $\lambda_1 = \lambda_2$ at $\phi = \pm\pi/2$. The beat effect may trigger the Arnold diffusion [46] since the full dynamics has the three degrees of freedom, (l_1, l_2, ϕ) (see, for example, Refs. [47, 48] for the recent progress on systems of three degrees of freedom). It will be interesting to observe evolution of the system in a very long time beyond the slow timescale $t_1 = \epsilon t$.

ACKNOWLEDGMENTS

Y.Y.Y. acknowledges the support of JSPS KAKENHI Grant Numbers 16K05472 and 21K03402. T.Y. acknowledges the support of JSPS KAKENHI Grant Numbers 18K03471 and 21K03411. T.K. is supported by Chubu University Grant (A). M.T. is supported by the Research Program of "Dynamic Alliance for Open Innovation Bridging Human, Environment and Materials" in "Network Joint Research Center for Materials and Devices", and a Grant-in-Aid for Scientific Research (C) (No. 22654047, 25610105, and 19K03653) from JSPS. The authors express their thanks to the anonymous referees who suggested to input the bending potential.

Appendix A: Lagrangians of the three-body bead-spring model

The system of Eq. (1) has the two-dimensional translational symmetry and the rotational symmetry. We reduce Eq. (1) and derive Eq. (2) by introducing the internal coordinates. For the reduction we perform three changes of variables.

The first change of variables introduces the vectors along the springs, denoted by \mathbf{q}_1 and \mathbf{q}_2 , with the center-of-mass \mathbf{q}_G . This change of variables is expressed as

$$\begin{pmatrix} \mathbf{q}_1 \\ \mathbf{q}_2 \\ \mathbf{q}_G \end{pmatrix} = \begin{pmatrix} -1 & 1 & 0 \\ 0 & -1 & 1 \\ m/M & m_2/M & m/M \end{pmatrix} \begin{pmatrix} \mathbf{r}_1 \\ \mathbf{r}_2 \\ \mathbf{r}_3 \end{pmatrix} \quad (\text{A1})$$

with the total mass

$$M = 2m + m_2. \quad (\text{A2})$$

Since each element of \mathbf{q}_G is a cyclic coordinate by an assumption and $\dot{\mathbf{q}}_G$ is conserved, we set $\dot{\mathbf{q}}_G \equiv \mathbf{0}$ without loss of generality. This setting reduces \mathbf{q}_G and $\dot{\mathbf{q}}_G$ from the Lagrangian, which is written as

$$L = \frac{1}{2} \sum_{i,j=1}^2 A^{ij} \dot{\mathbf{q}}_i \cdot \dot{\mathbf{q}}_j - V(\mathbf{q}_1, \mathbf{q}_2), \quad (\text{A3})$$

where we assumed that the potential energy function V depends on only \mathbf{q}_1 and \mathbf{q}_2 . A^{ij} is the (i, j) element of the size-2 matrix \mathbf{A} , which is defined by

$$\mathbf{A} = \begin{pmatrix} M_2 & M_1 \\ M_1 & M_2 \end{pmatrix}, \quad M_2 = \frac{m(m+m_2)}{M}, \quad M_1 = \frac{m^2}{M}. \quad (\text{A4})$$

The second change of variables introduces the polar coordinates (l_j, θ_j) , where l_j is the length of \mathbf{q}_j and θ_j is the angle of \mathbf{q}_j measured from a fixed direction on \mathbb{R}^2 . The vectors \mathbf{q}_j and $\dot{\mathbf{q}}_j$ are then written as

$$\mathbf{q}_j = l_j \mathbf{e}_{rj}, \quad \dot{\mathbf{q}}_j = \dot{l}_j \mathbf{e}_{rj} + l_j \dot{\theta}_j \mathbf{e}_{\theta j} \quad (\text{A5})$$

where \mathbf{e}_{rj} is the unit vector to the radial direction of \mathbf{q}_j , and $\mathbf{e}_{\theta j}$ is the unit vector to the angle direction.

As the third change of variables, we define

$$\phi = \theta_2 - \theta_1, \quad \psi = \theta_2 + \theta_1, \quad (\text{A6})$$

where ϕ represents the bending angle (see Fig. 1). The variables l_1, l_2, ϕ , and ψ describes the Lagrangian

$$L = \frac{1}{2} \sum_{\alpha, \beta=1}^4 B^{\alpha\beta}(\mathbf{z}) \dot{z}_\alpha \dot{z}_\beta - V(l_1, l_2, \phi) \quad (\text{A7})$$

where $\mathbf{z} = (z_1, z_2, z_3, z_4) = (l_1, l_2, \phi, \psi)$ and V does not depend on ψ by the assumption of rotational symmetry. The four-dimensional vector is represented by $\mathbf{z} \in \mathbb{R}^4$ to distinguish from the three-dimensional vector $\mathbf{y} \in \mathbb{R}^3$ used in Eq. (2). $B^{\alpha\beta}$ is the (α, β) element of the size-4 matrix \mathbf{B} . The matrix \mathbf{B} is symmetric, and we show only the upper triangle elements. The diagonal elements are

$$\begin{cases} B^{11} = B^{22} = M_2, \\ B^{33} = \frac{1}{4} M_2 (l_1^2 + l_2^2) - \frac{1}{2} M_1 l_1 l_2 \cos \phi, \\ B^{44} = \frac{1}{4} M_2 (l_1^2 + l_2^2) + \frac{1}{2} M_1 l_1 l_2 \cos \phi, \end{cases} \quad (\text{A8})$$

and the off-diagonal elements are

$$\begin{cases} B^{12} = M_1 \cos \phi, \\ B^{13} = B^{14} = -\frac{1}{2} M_1 l_2 \sin \phi, \\ B^{23} = -B^{24} = -\frac{1}{2} M_1 l_1 \sin \phi, \\ B^{34} = -\frac{1}{4} M_2 (l_1^2 - l_2^2). \end{cases} \quad (\text{A9})$$

The Lagrangian of Eq. (A7) does not depend on ψ and ψ is a cyclic coordinate. The conjugate momentum p_ψ , which corresponds to the total angular momentum, is defined by

$$p_\psi = \frac{\partial L}{\partial \dot{z}_4} = \sum_{\alpha=1}^4 B^{4\alpha} \dot{z}_\alpha \quad (\text{A10})$$

and is conserved. Eliminating $\dot{z}_4 (= \dot{\psi})$ from the kinetic energy, we obtain the Lagrangian

$$L = \frac{1}{2} \sum_{\alpha, \beta=1}^3 C^{\alpha\beta}(\mathbf{y}) \dot{y}_\alpha \dot{y}_\beta + \frac{[p_\psi(\mathbf{y}, \dot{\mathbf{y}})]^2}{2B^{44}(\mathbf{y})} - V(\mathbf{y}), \quad (\text{A11})$$

where we identified $\mathbf{B}(\mathbf{z})$ and $\mathbf{B}(\mathbf{y})$ since \mathbf{B} does not depend on ψ . Assuming $p_\psi = 0$, we obtain Eq. (2) because contribution from p_ψ to the Euler-Lagrange equation vanishes. The (α, β) element of the size-3 symmetric matrix \mathbf{C} is defined by

$$C^{\alpha\beta}(\mathbf{y}) = B^{\alpha\beta}(\mathbf{y}) - \frac{1}{B^{44}(\mathbf{y})} B^{4\alpha}(\mathbf{y}) B^{4\beta}(\mathbf{y}). \quad (\text{A12})$$

The diagonal elements are

$$\begin{cases} C^{11}(\mathbf{x}) = M_2 - \frac{M_1^2 l_2^2 \sin^2 \phi}{M_2 (l_1^2 + l_2^2) + 2M_1 l_1 l_2 \cos \phi}, \\ C^{22}(\mathbf{x}) = M_2 - \frac{M_1^2 l_1^2 \sin^2 \phi}{M_2 (l_1^2 + l_2^2) + 2M_1 l_1 l_2 \cos \phi}, \\ C^{33}(\mathbf{x}) = \frac{1}{4} M_2 (l_1^2 + l_2^2) - \frac{1}{2} M_1 l_1 l_2 \cos \phi \\ \quad - \frac{M_2^2 (l_1^2 - l_2^2)^2}{4M_2 (l_1^2 + l_2^2) + 8M_1 l_1 l_2 \cos \phi}, \end{cases} \quad (\text{A13})$$

and the off-diagonal elements are

$$\begin{cases} C^{12}(\mathbf{x}) = M_1 \cos \phi + \frac{M_1^2 l_1 l_2 \sin^2 \phi}{M_2 (l_1^2 + l_2^2) + 2M_1 l_1 l_2 \cos \phi}, \\ C^{13}(\mathbf{x}) = -\frac{1}{2} M_1 l_2 \sin \phi - \frac{\frac{1}{2} M_1 M_2 (l_1^2 - l_2^2) l_2 \sin \phi}{M_2 (l_1^2 + l_2^2) + 2M_1 l_1 l_2 \cos \phi}, \\ C^{23}(\mathbf{x}) = -\frac{1}{2} M_1 l_1 \sin \phi + \frac{\frac{1}{2} M_1 M_2 (l_1^2 - l_2^2) l_1 \sin \phi}{M_2 (l_1^2 + l_2^2) + 2M_1 l_1 l_2 \cos \phi}. \end{cases} \quad (\text{A14})$$

Appendix B: Kapitza pendulum

We review an analysis of the Kapitza pendulum. This review is adjusted to our theory for easily capturing a road map of long computations.

We consider a pendulum on the xy plane where the y axis points to the upward direction of the gravity g . The pendulum has the length l and a point mass m at the tip. The angle ϕ is taken from the downward direction of the y axis to the anti-clockwise direction. An external force oscillates the pivot of the pendulum along the y axis with the amplitude a and the frequency ω . The position (x, y) of the point mass is then written as

$$x = l \sin \phi, \quad y = -l \cos \phi - a \cos(\omega t + \delta), \quad (\text{B1})$$

where δ is the initial phase of the pivot. Constructing the Lagrangian, we have the Euler-Lagrange equation for ϕ as

$$\frac{d^2 \phi}{dt^2} = - \left[\left(\frac{\omega_0}{\omega} \right)^2 + \frac{a}{l} \cos(\bar{t} + \delta) \right] \sin \phi, \quad (\text{B2})$$

where $\omega_0 = \sqrt{g/l}$ and $\bar{t} = \omega t$. If no external oscillation is applied to the pivot, namely $a = 0$, the unique stable stationary point is clearly $\phi = 0$.

We assume that (i) the amplitude a of the oscillating pivot is much smaller than the pendulum length l and is of $O(\epsilon)$, (ii) the frequency ω_0 is much smaller than ω and is of $O(\epsilon)$, where ϵ is a dimensionless small parameter. These assumptions imply

$$\frac{a}{l} = \epsilon\alpha, \quad \frac{\omega_0}{\omega} = \epsilon\beta, \quad |\epsilon| \ll 1, \quad (\text{B3})$$

where α and β are of $O(\epsilon^0)$.

We introduce two timescales of

$$t_0 = \bar{t}, \quad t_1 = \epsilon\bar{t}, \quad (\text{B4})$$

which induce

$$\frac{d}{dt} = \frac{\partial}{\partial t_0} + \epsilon \frac{\partial}{\partial t_1}. \quad (\text{B5})$$

The angle ϕ is also expanded as

$$\phi(t) = \phi^{(0)}(t_1) + \epsilon\phi^{(1)}(t_0, t_1). \quad (\text{B6})$$

Substituting the above expansions into the Euler-Lagrange equation, Eq. (B2), we have the expanded equation

$$\begin{aligned} \epsilon^2 \frac{\partial^2 \phi^{(0)}}{\partial t_1^2} + \epsilon \frac{\partial^2 \phi^{(1)}}{\partial t_0^2} + 2\epsilon^2 \frac{\partial^2 \phi^{(1)}}{\partial t_0 \partial t_1} + \epsilon^3 \frac{\partial^2 \phi^{(1)}}{\partial t_1^2} \\ = - [\epsilon^2 \beta^2 + \epsilon\alpha \cos(t_0 + \delta)] \sin(\phi^{(0)} + \epsilon\phi^{(1)}). \end{aligned} \quad (\text{B7})$$

The equation to $O(\epsilon)$ is

$$\frac{\partial^2 \phi^{(1)}}{\partial t_0^2} = -\alpha \cos(t_0 + \delta) \sin \phi^{(0)}(t_1). \quad (\text{B8})$$

Solving the above equation with avoiding secular terms, we have

$$\phi^{(1)}(t_0, t_1) = \alpha \cos(t_0 + \delta) \sin \phi^{(0)}(t_1). \quad (\text{B9})$$

The equation to $O(\epsilon^2)$ is

$$\frac{\partial^2 \phi^{(0)}}{\partial t_1^2} + 2 \frac{\partial^2 \phi^{(1)}}{\partial t_0 \partial t_1} = - \left[\beta^2 \sin \phi^{(0)} + \alpha \phi^{(1)} \cos(t_0 + \delta) \cos \phi^{(0)} \right] \cdot \left(\frac{\partial V_{\text{bend}}}{\partial \phi} \right)^{(1)} = \frac{\partial^2 V_{\text{bend}}^{(0)}}{\partial \phi^2}(\phi^{(0)})\phi^{(1)} + \frac{\partial V_{\text{bend}}^{(1)}}{\partial \phi}(\phi^{(0)}). \quad (\text{B10}) \quad (\text{C4})$$

Substituting the $O(\epsilon)$ solution Eq. (B9) and averaging over the fast timescale t_0 , we have

$$\frac{\partial^2 \phi^{(0)}}{\partial t_1^2} = - \left(\beta^2 \sin \phi^{(0)} + \frac{\alpha^2}{4} \sin 2\phi^{(0)} \right). \quad (\text{B11})$$

The effective potential $V_{\text{eff}}(\phi^{(0)})$ satisfying

$$\frac{\partial^2 \phi^{(0)}}{\partial t_1^2} = - \frac{dV_{\text{eff}}}{d\phi^{(0)}}(\phi^{(0)}) \quad (\text{B12})$$

is then obtained as

$$V_{\text{eff}}(\phi^{(0)}) = - \left(\beta^2 \cos \phi^{(0)} + \frac{\alpha^2}{8} \cos 2\phi^{(0)} \right). \quad (\text{B13})$$

This effective potential has a local minimum at $\phi^{(0)} = \pi$ for $\alpha^2 > 2\beta^2$ in addition to $\phi^{(0)} = 0$. The inverted pendulum (i.e. $\phi = \pi$) is therefore stabilized by sufficiently fast oscillation (i.e. small β) of the pivot irrespective of the initial phase δ .

Appendix C: Order of the bending potential

We show $V_{\text{bend}}^{(0)}(\phi) \equiv 0$ and $V_{\text{bend}}^{(1)}(\phi) \equiv 0$ under the assumptions (A1) and (A2).

1. $O(\epsilon^0)$

There is no time derivative term in $O(\epsilon^0)$, and we have

$$\frac{\partial V_{\text{bend}}^{(0)}}{\partial \phi}(\phi^{(0)}) = 0. \quad (\text{C1})$$

The zeroth order term $V_{\text{bend}}^{(0)}$ is hence constant, and we can set $V_{\text{bend}}^{(0)}(\phi) \equiv 0$ without loss of generality. We note that the identical zero is induced because $\phi^{(0)}$ in Eq. (C1) is a variable. The spring potential V_{spring} is not identically zero in general because it is required to hold in $O(\epsilon^0)$

$$\frac{\partial V_{\text{spring}}}{\partial l_j}(l_*, l_*) = 0 \quad (j = 1, 2) \quad (\text{C2})$$

at the point $(l_1, l_2) = (l_*, l_*)$.

2. $O(\epsilon)$

The terms of $O(\epsilon)$ constructs

$$\mathbf{C}(\mathbf{y}^{(0)}) \frac{\partial^2}{\partial t_0^2} \begin{pmatrix} l_1^{(1)} \\ l_2^{(1)} \\ \phi^{(1)} \end{pmatrix} = \begin{pmatrix} -kl_1^{(1)} \\ -kl_2^{(1)} \\ -(\partial V_{\text{bend}}/\partial \phi)^{(1)} \end{pmatrix}, \quad (\text{C3})$$

where

The first term of the right-hand side in Eq. (C4) is zero since $V_{\text{bend}}^{(0)} \equiv 0$, and there is no restoring force for the variable $\phi^{(1)}$, while Eq. (C2) does not imply the zero restoring force for the springs. The second term $(\partial V_{\text{bend}}^{(1)}/\partial \phi)(\phi^{(0)})$ is constant in the timescale t_0 . If the second term is not zero, $\phi^{(1)}$ has a secular term, and the secular term breaks the perturbation expansion Eq. (10), which assumes $|\phi^{(0)}| \gg |\epsilon\phi^{(1)}|$. Therefore, the second term must be zero and we can set $V_{\text{bend}}^{(1)} \equiv 0$ without loss of generality.

Appendix D: Matrices in the equations of $O(\epsilon)$

We give the explicit forms of the matrix $\mathbf{X}(\mathbf{y}^{(0)})$ appearing in Eq. (15). The inverse matrix of \mathbf{C} at $\mathbf{y} = \mathbf{y}^{(0)}$ is

$$[\mathbf{C}(\mathbf{y}^{(0)})]^{-1} = \frac{1}{M_2^2 - M_1^2} \times \begin{pmatrix} M_2 & -M_1 \cos \phi^{(0)} & \frac{1}{l_*} M_1 \sin \phi^{(0)} \\ -M_1 \cos \phi^{(0)} & M_2 & \frac{1}{l_*} M_1 \sin \phi^{(0)} \\ \frac{1}{l_*} M_1 \sin \phi^{(0)} & \frac{1}{l_*} M_1 \sin \phi^{(0)} & \frac{2}{l_*^2} (M_2 + M_1 \cos \phi^{(0)}) \end{pmatrix}. \quad (\text{D1})$$

The matrix $\mathbf{X}(\mathbf{y}^{(0)}) = [\mathbf{C}(\mathbf{y}^{(0)})]^{-1} \mathbf{K}$ is hence

$$\mathbf{X}(\mathbf{y}^{(0)}) = \frac{k}{M_2^2 - M_1^2} \begin{pmatrix} M_2 & -M_1 \cos \phi^{(0)} & 0 \\ -M_1 \cos \phi^{(0)} & M_2 & 0 \\ \frac{1}{l_*} M_1 \sin \phi^{(0)} & \frac{1}{l_*} M_1 \sin \phi^{(0)} & 0 \end{pmatrix}. \quad (\text{D2})$$

Appendix E: Validity of the hypothesis

Under the equal mass condition $m_2 = m$, we examine validity of the hypothesis (H) expressed in Eq. (33). We introduce the approximations of

$$\frac{\partial l_j^{(1)}}{\partial t_0} \rightarrow \frac{dl_j}{dt}, \quad \phi^{(0)} \rightarrow \phi, \quad (\text{E1})$$

and the amplitudes of normal modes are expressed as

$$\begin{cases} w_1^2 = \frac{1}{2} \left[(l_1 + l_2 - 2l_*)^2 + \frac{1}{\lambda_1} (i_1 + i_2)^2 \right], \\ w_2^2 = \frac{1}{2} \left[(l_1 - l_2)^2 + \frac{1}{\lambda_2} (i_1 - i_2)^2 \right], \end{cases} \quad (\text{E2})$$

where the eigenvalues λ_1 and λ_2 are defined in Eq. (25). We compute the normal mode energy ratio defined by

$$R = \frac{E_1}{E_1 + E_2}, \quad E_j = \frac{k}{2} w_j^2 \quad (j = 1, 2). \quad (\text{E3})$$

The hypothesis is valid if R is constant in time.

We use the initial condition of Eq. (51) with $\phi_* = \pi/2$, and the amplitude of the normal modes is $w = 1.5$. Temporal evolution of R is exhibited in Fig. 7 for $\nu_1 = 1, 0.75, 0.5, 0.25$, and 0 with $\nu_2 = 1 - \nu_1$. The hypothesis (H) is valid around $\nu_1 = 1$ and 0 in particular.

Appendix F: Analysis of the effective potential V_{eff}

Let us study the critical points of the effective potential V_{eff} . A critical point is defined as the point at which $V'_{\text{eff}} = 0$. The derivative of V_{eff} is

$$V'_{\text{eff}}(\phi) = M_{\text{eff}}(\phi) G_\nu(\phi). \quad (\text{F1})$$

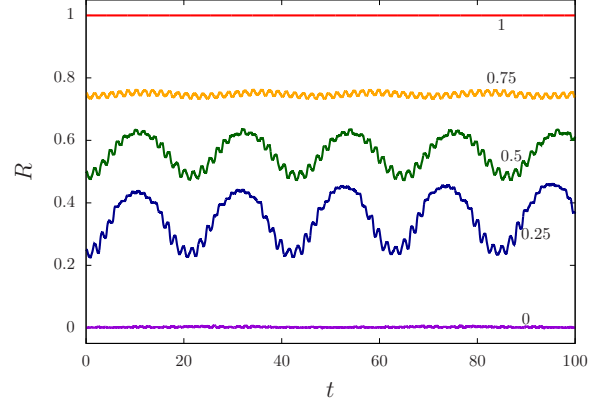


FIG. 7. Temporal evolution of the normal mode energy ratio R . $\nu_1 = 1.0$ (red), 0.75 (orange), 0.5 (green), 0.25 (blue), and 0 (magenta) from top to bottom. The amplitude of the normal modes is $w = 1.5$.

Thus, we have

$$\phi \text{ is a critical point} \iff G_\nu(\phi) = 0 \quad (\text{F2})$$

since the effective mass M_{eff} is always positive as found in Eq. (45). The effective potential at a critical point takes a local minimum or a local maximum depending on the sign of the second derivative. At a critical point, we have $G_\nu = 0$ and the second derivative of V_{eff} is

$$\phi \text{ is a critical point} \implies V''_{\text{eff}}(\phi) = M_{\text{eff}}(\phi) G'_\nu(\phi). \quad (\text{F3})$$

Again from $M_{\text{eff}} > 0$, the sign of V''_{eff} is determined by the sign of G'_ν . Keeping in mind the above discussions, we study the critical points of the effective potential for absence and appearance of the bending potential.

1. Absence of the bending potential

The function G_ν is proportional to T_ν for $V_{\text{bend}} \equiv 0$, and the sinusoidal function in T_ν gives the two critical points of $\phi = 0$ and π . In addition, there are the other two possible critical points $\phi = \pm\phi_\#$ which solve the equation

$$\frac{\nu_1}{M_2 - M_1 \cos \phi} - \frac{\nu_2}{M_2 + M_1 \cos \phi} = 0 \quad (\text{F4})$$

with $\nu_2 = 1 - \nu_1$ and exist in the interval

$$\frac{M_2 - M_1}{2M_2} < \nu_1 < \frac{M_2 + M_1}{2M_2}. \quad (\text{F5})$$

The derivatives of G_ν at $\phi = 0$ and π are respectively

$$G'_\nu(0) = \frac{E^{(2)}}{l_*^2} \frac{M_1}{M_2 - M_1} \frac{(2\nu_1 - 1)M_2 + M_1}{M_2^2 - M_1^2} \quad (\text{F6})$$

and

$$G'_\nu(\pi) = \frac{E^{(2)}}{l_*^2} \frac{M_1}{M_2 + M_1} \frac{(1 - 2\nu_1)M_2 + M_1}{M_2^2 - M_1^2}, \quad (\text{F7})$$

where we used the relation $\nu_2 = 1 - \nu_1$. The point $\phi = 0$ is hence a local minimum point ($V_{\text{eff}}''(0) > 0$) if and only if

$$\nu_1 > \frac{M_2 - M_1}{2M_2}, \quad (\text{F8})$$

and the point $\phi = \pi$ is a local minimum point ($V_{\text{eff}}''(\pi) > 0$) if and only if

$$\nu_1 < \frac{M_2 + M_1}{2M_2}. \quad (\text{F9})$$

The two points $\phi = 0$ and $\phi = \pi$ are the local minimum points in the interval of Eq. (F5). The periodicity of the effective potential $V_{\text{eff}}(\phi)$ requires the same numbers of local minimum points ($V_{\text{eff}}'' > 0$) and local maximum points ($V_{\text{eff}}'' < 0$), and hence the critical points $\phi = \pm\phi_{\#}$ are the local maximum points.

2. Appearance of the bending potential

We write the function $G_{\nu}(\phi)$ as

$$G_{\nu}(\phi) = \frac{\sin \phi}{l_*^2(M_2 - M_1 \cos \phi)} g_{\nu_1}(\phi) \quad (\text{F10})$$

where

$$g_{\nu_1}(\phi) = -8 \cos \phi + (E^{(2)} - \cos 2\phi - 1) \times \left[\frac{\nu_1}{M_2 - M_1 \cos \phi} - \frac{\nu_2}{M_2 + M_1 \cos \phi} \right]. \quad (\text{F11})$$

The effective potential has the critical points at $\phi = 0, \pi$, and $\phi_{\#}$ satisfying $g(\phi_{\#}) = 0$. We separately discuss the second derivative

$$V_{\text{eff}}''(\phi) = g_{\nu_1}(\phi) \frac{\partial}{\partial \phi} \left[\frac{\sin \phi}{l_*^2(M_2 - M_1 \cos \phi)} \right] + \frac{\sin \phi}{l_*^2(M_2 - M_1 \cos \phi)} g'_{\nu_1}(\phi) \quad (\text{F12})$$

at a critical point.

a. The critical points $\phi = 0$ and π

The second term of the right-hand side of Eq. (F12) is zero, and

$$\frac{\partial}{\partial \phi} \left[\frac{\sin \phi}{l_*^2(M_2 - M_1 \cos \phi)} \right] = \frac{\cos \phi}{l_*^2(M_2 - M_1 \cos \phi)}. \quad (\text{F13})$$

This factor is positive (negative) at $\phi = 0$ (π), and the sign of V_{eff}'' is determined by $g_{\nu_1}(\phi)$. We have

$$g_{\nu_1}(0) = -8 + (E^{(2)} - 2) \frac{M_1 M_2}{M_2^2 - M_1^2} \left(2\nu_1 - 1 + \frac{M_1}{M_2} \right) \quad (\text{F14})$$

and

$$g_{\nu_1}(\pi) = 8 + (E^{(2)} - 2) \frac{M_1 M_2}{M_2^2 - M_1^2} \left(2\nu_1 - 1 - \frac{M_1}{M_2} \right). \quad (\text{F15})$$

We separately discuss for $0 \leq E^{(2)} \leq 2$ and $E^{(2)} > 2$, where the boundary $E^{(2)} = 2$ comes from the bending potential at $\phi = 0$ and π : $V_{\text{bend}}^{(2)}(0) = V_{\text{bend}}^{(2)}(\pi) = 2$.

If $0 \leq E^{(2)} \leq 2$, the maximum value of $g_{\nu_1}(0)$ is realized at $\nu_1 = 0$, which gives

$$g_0(0) = -8 + (2 - E^{(2)}) \frac{1 - 1/(M_2/M_1)}{M_2/M_1 - 1/(M_2/M_1)} < -7 \quad (\text{F16})$$

for $0 \leq E^{(2)} \leq 2$. Note $M_2/M_1 > 1$. The point $\phi = 0$ is hence a local maximum point for $0 \leq E^{(2)} \leq 2$. A similar discussion states that the point $\phi = \pi$ is a local maximum point for $0 \leq E^{(2)} \leq 2$.

For $E^{(2)} > 2$, the effective potential takes a local minimum at $\phi = 0$ if

$$\nu_1 > \frac{1}{2} \left(1 - \frac{1}{M_2/M_1} \right) + \frac{4}{E^{(2)} - 2} \left(\frac{M_2}{M_1} - \frac{1}{M_2/M_1} \right), \quad (\text{F17})$$

and takes a local minimum at $\phi = \pi$ if

$$\nu_1 < \frac{1}{2} \left(1 + \frac{1}{M_2/M_1} \right) - \frac{4}{E^{(2)} - 2} \left(\frac{M_2}{M_1} - \frac{1}{M_2/M_1} \right). \quad (\text{F18})$$

By changing the inequalities into the equality, Eq. (F17) gives the red dotted-line and Eq. (F18) gives the blue dashed-line in Figs. 4 and 5. We remark that Eq. (F18) is equivalent with

$$\nu_2 > \frac{1}{2} \left(1 - \frac{1}{M_2/M_1} \right) + \frac{4}{E^{(2)} - 2} \left(\frac{M_2}{M_1} - \frac{1}{M_2/M_1} \right), \quad (\text{F19})$$

whose right-hand side is identical with that of Eq. (F17).

b. The critical point $\phi = \phi_{\#}$

We have $g(\phi_{\#}) = 0$, and

$$V_{\text{eff}}''(\phi_{\#}) = \frac{\sin \phi_{\#}}{l_*^2(M_2 - M_1 \cos \phi_{\#})} g'(\phi_{\#}). \quad (\text{F20})$$

The effective potential takes a local minimum (maximum) if $V_{\text{eff}}''(\phi_{\#}) > 0$ ($V_{\text{eff}}''(\phi_{\#}) < 0$) at the critical point $\phi_{\#}$.

Appendix G: Explanation on movies

We provide movies for the initial conformations shown in Fig. 8 in Supplemental Material [43]. The bending potential $V_{\text{bend}}^{(2)}(\phi)$ of Eq. (48) is in use. The excited spring mode is $(\nu_1, \nu_2) = (1, 0)$, and the amplitude w is

$w = 0.5$ for Figs. 8 (a) and (d), $w = 1$ for (b) and (e), and $w = 1.5$ for (c) and (f). The other initial conditions are described in Sec. VB, and the system parameter values (m_i , k , and l_*) are given in Sec. VA. Dynamics of the system corresponding to the panels from Figs. 8(a) to (f) is demonstrated in from MovieA to MovieF, respectively. We stress that temporal evolution is well understood by the effective potential V_{eff} , while the bending potential [see Fig. 3(a)] does not explain it.

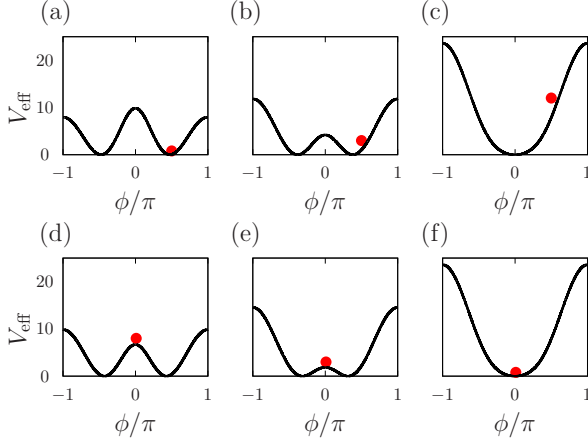


FIG. 8. Initial conformations (red points) and effective potentials (black lines). The reference conformations are $\phi_* = \pi/2$ in the panels (a), (b), and (c), and $\phi_* = 0.01$ in (d), (e), and (f), where the initial conformation ϕ_0 is close to ϕ_* . See Figs. 6(d), (e), and (f) for temporal evolution of $\phi(t)$ corresponding to the panels (a), (b), and (c), respectively.

Appendix H: From a general potential to the bending potential

The bending potential $V_{\text{bend}}(\phi)$ represents the interaction between the two beads of the ends, because the interaction between an end and the center beads results in the spring potential. We show that the bending potential energy function of ϕ is derived from any potential V_G which is a function of the distance $r = \|\mathbf{r}_3 - \mathbf{r}_1\|$, although it is assumed to be a function of only ϕ in the main text. Here r is represented by using l_1 , l_2 , and ϕ as

$$r = \|(\mathbf{r}_3 - \mathbf{r}_2) + (\mathbf{r}_2 - \mathbf{r}_1)\| = \sqrt{l_1^2 + l_2^2 + 2l_1l_2 \cos \phi}. \quad (\text{H1})$$

Substituting Eq. (9) into Eq. (H1), we have $r = r^{(0)} + O(\epsilon)$ and

$$r^{(0)} = l_* \sqrt{2(1 + \cos \phi^{(0)})}. \quad (\text{H2})$$

As shown in Appendix C, the potential V_G is of $O(\epsilon^2)$ under the assumptions (A1) and (A2), and we expand it as

$V_G(r) = \epsilon^2 V_G^{(2)}(r) + O(\epsilon^3) = \epsilon^2 V_G^{(2)}(r^{(0)}) + O(\epsilon^3)$. (H3)
Therefore, the second order bending potential $V_{\text{bend}}^{(2)}$ is derived as a function of only $\phi^{(0)}$ as

$$V_{\text{bend}}^{(2)}(\phi^{(0)}) = V_G^{(2)}\left(l_* \sqrt{2(1 + \cos \phi^{(0)})}\right). \quad (\text{H4})$$

The effective potential V_{eff} is obtained from Eq. (46) by substituting the above bending potential $V_{\text{bend}}^{(2)}$ into Eq. (42).

-
- [1] D. Koshland, Application of a theory of enzyme specificity to protein synthesis, *Proc. Natl. Acad. Sci. USA* **44**, 98 (1958).
 - [2] J. Monod, J. Wyman, and J. P. Changeux, On the nature of allosteric transitions: A plausible model, *J. Mol. Biol.* **12**, 88 (1965).
 - [3] K. Okazaki and S. Takada, Dynamic energy landscape view of coupled binding and protein conformational change: Induced-fit versus population-shift mechanisms, *PNAS* **105**, 11182 (2008).
 - [4] D. Seeliger and B. L. de Groot, Conformational transitions upon ligand binding: Holo structure prediction from apo conformations, *PLoS Comput. Biol.* **6**, e1000634 (2010).
 - [5] S. Fuchigami, H. Fujisaki, Y. Matsunaga, and A. Kidera, Protein functional motions: Basic concepts and computational methodologies, in *Advancing theory for kinetics and dynamics of complex, many-dimensional systems: Clusters and Proteins: Advances in Chemical Physics, Volume 145* (Wiley, New Jersey, 2011).
 - [6] H. Hauser, A. J. Ijspeert, R. M. Fuchsli, R. Pfeifer, and W. Maass, Towards a theoretical foundation for morphological computation with compliant bodies, *Biol. Cybern.* **105**, 355 (2011).
 - [7] Special issue on Morphological Computation, *Artificial Life* **19**(1) (2013).
 - [8] V. C. Müller and M. Hoffmann, What Is Morphological Computation? On How the Body Contributes to Cognition and Control, *Artificial Life* **23**, 1 (2017).
 - [9] S. Collins, A. Ruina, R. Tedrake, and M. Wisse, Efficient bipedal robots based on passive-dynamic walkers, *Science* **307**, 1082 (2005).
 - [10] M. Hermans, B. Schrauwen, P. Bienstman, and J. Dambre, Automated design of complex dynamic systems, *PLoS ONE* **9**, e86696 (2014). doi:10.1371/journal.pone.0086696
 - [11] J. U. Surjadi, L. Gao, H. Du, X. Li, X. Xiong, N. X. Fang, and Y. Lu, Mechanical metamaterials and their engineering applications, *Adv. Eng. Mater.* **21**, 1800864 (2019).
 - [12] Z. Y. Wei, Z. V. Guo, L. Dudte, H. Y. Liang, and L. Mahadevan, Geometric mechanics of periodic pleated origami, *Phys. Rev. Lett.* **110**, 215501 (2013).
 - [13] A. Stephenson, XX. On induced stability, *The Lon-*

- don, Edinburgh, and Dublin Philosophical Magazine and Journal of Science **15**, 233 (1908).
- [14] P. L. Kapitza, Dynamic stability of a pendulum when its point of suspension vibrates, Soviet Phys. JETP **21**, 588 (1951); Collected papers of P. L. Kapitza, Vol.2, pp.714–737 (1965).
- [15] P. E. Rouse, A theory of the linear viscoelastic properties of dilute solutions of coiling polymers, J. Chem. Phys. **21**, 1272 (1953).
- [16] B. H. Zimm, Dynamics of polymer molecules in dilute solution: Viscoelasticity, flow birefringence and dielectric loss, J. Chem. Phys. **24**, 269 (1956).
- [17] E. Gauger and H. Stark, Numerical study of a microscopic artificial swimmer, Phys. Rev. E **74**, 021907 (2006).
- [18] Y. Mirzae, B. Y. Rubinstein, K. I. Morozov, and A. M. Leshansky, Modeling propulsion of soft magnetic nanowires, Front. Robot. AI **7**, 595777 (2020).
- [19] A. Saadat and B. Khomami, A new bead-spring model for simulation of semi-flexible macromolecules, J. Chem. Phys. **145**, 024902 (2016).
- [20] M. Bukov, L. D’Alessio, and A. Polkovnikov, Universal high-frequency behavior of periodically driven systems: from dynamical stabilization to Floquet engineering, Advances in Physics **64**, 139 (2015).
- [21] M. Grifoni and P. Hänggi, Coherent and incoherent quantum stochastic resonance, Phys. Rev. Lett. **76**, 1611 (1996).
- [22] A. Wickenbrock, P. C. Holz, N. A. Abdul Wahab, P. Phoonthong, D. Cubero, and F. Renzoni, Vibrational mechanics in an optical lattice: Controlling transport via potential renormalization. Phys. Rev. Lett. **108**, 020603 (2012).
- [23] V. N. Chizhevsky, E. Smeu, and G. Giacomelli, Experimental evidence of “vibrational resonance” in an optical system, Phys. Rev. Lett. **91**, 220602 (2003).
- [24] V. N. Chizhevsky, Experimental evidence of vibrational resonance in a multistable system, Phys. Rev. E **89**, 062914 (2014).
- [25] D. Cubero, J. P. Baltanas, and J. Casado-Pascual, High-frequency effects in the Fitzhugh-Nagumo neuron model, Phys. Rev. E **73**, 061102 (2006).
- [26] M. Bordet and S. Morfu, Experimental and numerical study of noise effects in a FitzHugh–Nagumo system driven by a biharmonic signal, Chaos, Solitons & Fractals **54**, 82 (2013).
- [27] S. H. Weinberg, High frequency stimulation of cardiac myocytes: A theoretical and computational study, Chaos **24**, 043104 (2014).
- [28] M. Uzuntarla, E. Yilmaz, A. Wagemakers, and M. Ozer, Vibrational resonance in a heterogeneous scale free network of neurons, Commun. Nonlinear Sci. Numer. Simulat. **22**, 367 (2015).
- [29] R. H. Buchanan, G. Jameson, and D. Oedjoe, Cyclic migration of bubbles in vertically vibrating liquid columns, Ind. Eng. Chem. Fund. **1**, 82 (1962).
- [30] M. H. I. Baird, Resonant bubbles in a vertically vibrating liquid column, Can. J. Chem. Eng. **41**, 52 (1963).
- [31] G. J. Jameson, The motion of a bubble in a vertically oscillating viscous liquid, Chem. Eng. Sci. **21**, 35 (1966).
- [32] B. Apffel, F. Novkoski, A. Eddi, and E. Fort, Floating under a levitating liquid, Nature **585**, 48 (2020).
- [33] R. E. Bellman, J. Bentsman, and S. M. Meerkov, Vibrational control of nonlinear systems, IEEE Trans. Automat. Contr. **31**, 710 (1986).
- [34] B. Shapiro and B. T. Zinn, High-frequency nonlinear vibrational control, IEEE Trans. Automat. Contr. **42**, 83 (1997).
- [35] M. Borromeo and F. Marchesoni, Artificial sieves for quasimassless particles, Phys. Rev. Lett. **99**, 150605 (2007).
- [36] C. J. Richards, T. J. Smart, P. H. Jones, and D. Cubero, A microscopic Kapitza pendulum, Scientific Reports **8**, 13107 (2018).
- [37] C. M. Bender and S. A. Orszag, Advanced Mathematical Methods for Scientists and Engineers I: Asymptotic Methods and Perturbation Theory (Springer, 1999).
- [38] N. M. Krylov and N. N. Bogoliubov, New Methods of Nonlinear Mechanics in their Application to the Investigation of the Operation of Electronic Generators. I (United Scientific and Technical Press, Moscow, 1934).
- [39] N. M. Krylov and N. N. Bogoliubov, Introduction to Nonlinear Mechanics (Princeton University Press, Princeton, 1947).
- [40] J. Guckenheimer and P. Holmes, Nonlinear Oscillations, Dynamical Systems, and Bifurcations of Vector Fields (Springer-Verlag, New York, 1983).
- [41] T. Yanagita and T. Konishi, Numerical analysis of new oscillatory mode of bead-spring model, Journal of JSCE A2 **75**, I.125 (2019) (in Japanese).
- [42] H. Yoshida, Construction of higher order symplectic integrators, Phys. Lett. A **190**, 262 (1990).
- [43] See Supplemental Material at [URL] for movies.
- [44] Y. Y. Yamaguchi, T. Yanagita, T. Konishi, and M. Toda, Dynamically induced conformation depending on excited normal modes of fast oscillation, arXiv:2111.10025v1.
- [45] Y. Y. Yamaguchi, in preparation.
- [46] V. I. Arnold, Instability of dynamical systems with several degrees of freedom, Sov. Math.-Dokl. **5**, 58 (1964).
- [47] P. Manikandan and S. Keshavamurthy, Dynamical traps lead to the slowing down of intramolecular vibrational energy flow, PNAS **111**, 14354 (2014).
- [48] M. Firmbach, S. Lange, R. Ketzmerick, and A. Bäcker, Three-dimensional billiards: Visualization of regular structures and trapping of chaotic trajectories, Phys. Rev. E **98**, 022214 (2018).